Rapid Communications

Detection of multipolar orders in the spin-orbit-coupled 5*d* Mott insulator Ba_2MgReO_6

Daigorou Hirai,[1,*] Hajime Sagayama,[2] Shang Gao,[3,†] Hiroyuki Ohsumi,[4] Gang Chen,[5,6] Taka-hisa Arima,[3,7] and Zenji Hiroi[1]

[1]*Institute for Solid State Physics, University of Tokyo, Kashiwa, Chiba 277-8581, Japan*
[2]*Institute of Materials Structure Science, High Energy Accelerator Research Organization, Tsukuba, Ibaraki 305-0801, Japan*
[3]*RIKEN Center for Emergent Matter Science, Wako 351-0198, Japan*
[4]*RIKEN SPring-8 Center, Sayo 679-5148, Japan*
[5]*Department of Physics, Center of Theoretical and Computational Physics, the University of Hong Kong, Hong Kong, China*
[6]*Department of Physics, State Key Laboratory of Surface Physics, Fudan University, Shanghai 200433, China*
[7]*Department of Advanced Materials Science, University of Tokyo, Kashiwa 277-8561, Japan*

(Received 17 February 2020; revised manuscript received 23 April 2020; accepted 28 April 2020; published 17 June 2020)

Synchrotron x-ray-diffraction measurements on single crystals of the double perovskite Ba_2MgReO_6 with $5d^1$ electronic configurations reveal the successive phase transitions from a disordered state to a quadrupolar order at $T_q = 33$ K, and then, to a dipolar ordered state at $T_m = 18$ K. The magnetic reflections observed below T_m are indexed to a propagation vector with $k = [0\ 0\ 1]$, indicating a canted antiferromagnetic order. The very small deformation of ReO_6 octahedra observed below T_q demonstrates that the quadrupolar order is composed of antiferroically arranged $Q_{x^2-y^2}$ and ferroically arranged $Q_{3z^2-r^2}$ moments. These observations are consistent with the mean-field theory for spin-orbit-entangled electrons. Our findings are a significant step towards understanding the intriguing physics of multipoles realized by spin-orbit-entangled 5*d* electrons.

DOI: 10.1103/PhysRevResearch.2.022063

Exotic quantum phases, such as high-temperature superconductivity [1,2], colossal magnetoresistance [3,4], and heavy Fermion states [5,6] are observed in materials with strong electron-electron correlations, and both the spin and the orbital degrees of freedom of an electron are thought to play an important role. In particular, strong interactions between spin and orbital moments—an effect known as spin-orbit interactions (SOIs)—are expected to produce a variety of exotic phenomena [7–9].

In this context, over the past ten years, research has focused on heavy transition-metal (TM) compounds [7–9] where the combined effect of electron correlations and SOIs is realized. For example, in Sr_2IrO_4, a spin-orbit-entangled Mott insulating state emerges as a result of electron correlation effectively enhanced by SOIs [10,11]. When these spin-orbit-entangled electrons interact with each other, a novel quantum phase called the Kitaev spin liquid occurs [9,12]. Moreover, exotic topological phases can emerge when the spin-orbit-entangled electrons begin to delocalize [7,8]. Despite these intriguing phenomena, the understanding of 5*d* electron systems remains incomplete. In particular, the multipolar order [13,14] has not yet been experimentally well established. The electrons with strong spin-orbital entanglement may experience various symmetry-breaking transitions, which can be described by multipole moments [15]. The higher-order multipolar order is generally subtle and hard to detect by traditional experimental probes in comparison to conventional dipolar orders; this is why the multipolar order is also known as the "hidden order" [16,17]. In addition, model 5*d* materials that can demonstrate the characteristics of multipolar orders are lacking thus far.

There are two requirements to create a multipolar order in an actual material. One is a high local symmetry at the TM site, which leads to an unquenched orbital moment. The other is an appropriate distance and charge transfer between TM ions for electrons to be localized; many 5*d* TM compounds are weakly correlated metals with relatively large bandwidths. In terms of these requirements, double-perovskite (DP) compounds [18] are good candidates as they comprise octahedrally coordinated TM ions that are spatially separated from each other. Thus far, several DP compounds have been suggested by both theoretically [8,13,19] and experimentally to exhibit multipolar order: Ba_2NaOsO_6 [20–23], Ba_2YMoO_6 [24], Ba_2MgReO_6 [25,26], Ba_2MOsO_6 (M = Zn, Mg, and Ca) [27], and A_2TaCl_6 (A = Rb, and Cs) [28]. A recent nuclear magnetic resonance study revealed that Ba_2NaOsO_6 shows a noncollinear spin order and a small structural distortion, which was suggested to be due to a quadrupolar order [22]. Moreover, ferro-octupolar order was suggested for Ba_2MOsO_6 (M = Zn, Mg, and Ca) based on the observation of a gapped magnetic excitation spectrum without additional magnetic Bragg peaks [27].

*dhirai@issp.u-tokyo.ac.jp
†Present address: Materials Science & Technology Division and Neutron Science Division, Oak Ridge National Laboratory, Oak Ridge, Tennessee 37831, USA.

We focus on Ba_2MgReO_6 [25,26,29] which crystallizes in a DP (elpasolite) structure with a face-centered-cubic lattice in the space-group $Fm\bar{3}m$. The Re^{6+} ion possesses a $5d^1$ electron configuration and adopts a spin-orbit-entangled $J_{\rm eff} = 3/2$ quartet as the ground state [30]. Upon cooling, Ba_2MgReO_6 undergoes two phase transitions at $T_q = 33$ and $T_m = 18$ K [25,26]. In the magnetically ordered phase below T_m, an exotic spin structure is inferred from the small saturation moment of $0.3\,\mu_B$ and an unusual easy axis along the [1 1 0] direction [26]. These magnetic behaviors are very similar to those observed in Ba_2NaOsO_6 [22]. Thus, a quadrupolar order is expected to occur at high temperatures above T_m. However, the nature of the intermediate phase between T_q and T_m remains unknown. In particular, key evidence for the quadrupolar order, such as a structural change accompanied by the quadrupolar order, has not yet been detected in previous neutron-diffraction measurements on polycrystalline samples [25].

Here, we show the experimental results of state-of-the-art synchrotron x-ray-diffraction (XRD) measurements on Ba_2MgReO_6. We have successfully observed orderings of both magnetic dipoles at $T_m = 18$ K and charge quadrupoles at $T_q = 33$ K and unambiguously determined their patterns. This compound provides us with an opportunity to study quantum phases appearing among strongly correlated electrons with strong SOIs.

High-quality single crystals of Ba_2MgReO_6 were grown by the flux method as reported before [26]. Resonant XRD experiments were performed on BL19LXU at SPring-8 [31]. A Ba_2MgReO_6 single crystal with dimensions of $2 \times 2 \times 1\,\text{mm}^3$ was fixed to a ^{4}He closed-cycle refrigerator mounted on a four-circle diffractometer. Off-resonant XRD experiments were performed on the beamlines BL-8A and AR-NE1A in the High Energy Accelerator Research Organization. An incident x ray with wavelength $\lambda = 0.690$ Å was used at BL-8A and high-flux and short-wavelength x-ray beams with $\lambda = 0.418$ Å were used at AR-NE1A in order to detect weak superlattice reflections. XRD intensities were collected by the oscillation photograph technique using a large cylindrical image plate to index Bragg reflections and integrating their intensities.

To reveal the characteristics of the successive phase transitions in Ba_2MgReO_6, we employed two kinds of XRD techniques. First, the magnetic order below T_m has been investigated in terms of the resonant effect at the x-ray absorption edge, which is generally superior in determining the ordered structures of small dipole moments using small single crystals [11,32–34]. Second, structural changes across the two transitions at T_q and T_m are examined by nonresonant XRD experiments to probe the quadrupolar order and its influence on the magnetic order. The very small structural change accompanied by the quadrupolar order, which is approximately one order of magnitude smaller than that induced by the orbital order in $3d$ electron systems [35,36], can only be detected with an ultra-high-intensity synchrotron x-ray beam using high-crystallinity samples.

Figure 1(a) shows a typical XRD profile taken below T_m at 6 K for the $(1\,0\,0)_t$ reflection which is not allowed for the body-centered-tetragonal lattice attained below T_q as described later; the subscripts t and c denote the index based on the tetragonal and cubic cells, respectively. The peak is strongly enhanced at around the Re $L_{\rm III}$ absorption edge of 10.535 keV (excitation from the $2p_{3/2}$ state to the $5d$ state), indicative of its magnetic origin. Moreover, polarization analysis (see the Supplemental Material [37]) shows that the reflection appears not in the σ-σ' channel but in the σ-π' channel, further confirming that it is a magnetic reflection. This $(1\,0\,0)_t$ magnetic reflection appears only below 18 K [Fig. 1(b)], indicating that the dipole moments of Re arranged below T_m.

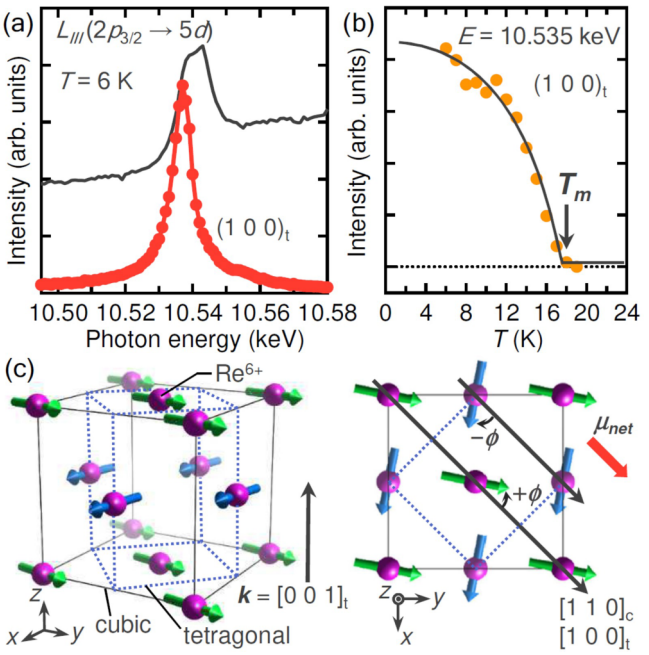

FIG. 1. (a) Photon-energy dependence of the $(1\,0\,0)_t$ magnetic reflection intensity (red circles) and the x-ray fluorescence spectrum (solid line) measured below T_m at 6 K. The subscripts "t" and "c" denote the index based on the tetragonal and cubic cells shown in (c). (b) Temperature dependence of the intensity of the $(1\,0\,0)_t$ reflection (orange circles), which increases below $T_m = 18$ K. The black line is a visual guide. (c) Proposed magnetic structure with a propagation vector of $\boldsymbol{k} = [0\,0\,1]_t$. Magnetic moments on the two sublattices are distinguished by colors, green at $z = 0$ and blue at $z = 1/2$. The high-temperature face-centered-cubic and low-temperature primitive tetragonal unit cells are depicted by solid and dotted lines, respectively.

We observe four magnetic reflections exhibiting resonance enhancement in our resonant XRD experiments (see the Supplemental Material [37]), all of which can be indexed with a single propagation vector with $\boldsymbol{k} = [0\,0\,1]_t$. This propagation vector indicates a two-sublattice magnetic structure with the spins aligning ferromagnetically within the $(0\,0\,1)_t$ plane and with the layers stacking antiferromagnetically along the $[0\,0\,1]_t$ direction. Thus, the observed net moments must be parasitic, arising from spin canting. Considering the easy-axis anisotropy along the $[1\,1\,0]_c$ direction in the cubic structure [26], we propose a possible spin structure as depicted in Fig. 1(c): The spins on the $z = 0$ plane rotate from $[1\,1\,0]_c$, which corresponds to $[1\,0\,0]_t$, by an angle of $+\phi$ and those on the $z = 1/2$ plane rotate by $-\phi$ so that an uncompensated

moment remains along $[1\ 1\ 0]_c$. This canted antiferromagnetic spin structure is essentially the same as that theoretically predicted for the spin-orbit-entangled d^1 electron system in DPs [13,38] and observed for Ba_2NaOsO_6 [22]. The canting angle is large: $\phi \sim 40^\circ$ for Ba_2MgReO_6 [26] and 67° for Ba_2NaOsO_6 [22]. The origin of this unusual magnetic order may be related to the theoretically predicted quadrupolar order above T_m.

Next, we investigated the nature of the phase transition at $T_q = 33$ K using the nonresonant synchrotron XRD technique. As summarized in Fig. 2 (also in the Supplemental Material [37]), a clear cubic-to-tetragonal structural transition is observed at T_q, which is evidenced by a split of the $(0\,0\,24)_c$ Bragg peak [Fig. 2(b)]. The relation between the high-temperature cubic and the low-temperature tetragonal unit cells is depicted in Fig. 1(c). As shown in Fig. 2(c), the tetragonal distortion $(c_t - \sqrt{2}a_t)$ develops gradually below T_q, leading to a very small distortion of ~0.09% at 25 K. Note that the tetragonal distortion is further enhanced upon cooling below T_m. The distortion in Ba_2MgReO_6 is much smaller than in other DPs, for example, ~0.47% in Ba_2CaWO_6 [39].

In addition to the split of fundamental reflections, 141 additional (superlattice) reflections, which are extremely weak (less than 0.005% of the strongest fundamental reflection), are detected below T_q in our nonresonant x-ray-diffraction experiments. The evolution of intensity over temperature of a superlattice reflection $(4\ 1\ 0)_t$ is shown in Fig. 2(d), appearing at T_q and increasing gradually with increasing tetragonal distortion. Then, the intensity starts to decrease at approximately T_m, which is in contrast to the further increase in the tetragonal distortion below T_m. We observe no additional superlattice reflections below T_m, suggesting no additional changes in the crystal structure. Reflection conditions of $0\ 0\ l$: $l = 2n$, $h\ 0\ 0$: $h = 2n$, and $0\ k\ l$: $k + l = 2n$ are observed for the superlattice reflections (Supplemental Material [37]), suggesting the tetragonal space groups that are possible, namely, $P4_2/mnm$ (136), $P\bar{4}n2$ (118), and $P4_2nm$ (102). Note that none of these space groups are observed for other DP compounds [18], indicating the unique structural distortion below T_q.

We consider atomic displacements in the intermediate phase from a high-symmetry tetragonal space group $I4/mmm$ (details are described in the Supplemental Material [37]). Among the possible space groups, only $P4_2/mnm$ belongs to the maximal nonisomorphic subgroups of $I4/mmm$; the other possible space groups of $P\bar{4}n2$ and $P4_2nm$ are the maximal nonisomorphic subgroups of $P4_2/mnm$ [40]. Our refinement reveals that space-group $P4_2/mnm$ provides a satisfactory fit, whereas a further symmetry lowering in the $P\bar{4}n2$ or $P4_2nm$ space group does not improve the fit. This model accurately reproduces the intensities of all the observed (141) superlattice reflections as well as those of the fundamental reflections (as shown in the Supplemental Material [37]). In the tetragonal $P4_2/mnm$ structure, from the high-temperature cubic $Fm\bar{3}m$ structure, a single type of oxygen site splits into three types of oxygen sites, an apical site O1 at $4e$ and in-plane sites O2 at $4f$ and O3 at $4g$ as illustrated in Fig. 2(e). This site splitting causes a slight elongation of the ReO_6 octahedron in the c direction and a rhomboid ε_v-type distortion of the square formed by four oxygens surrounding the Re ion on the (0 0 1) plane. The displacement of O1 from the regular octahedron (δz at 6 K ~0.007 Å) corresponds to approximately half of the tetragonal distortion; $(c_t - \sqrt{2}a_t)/2$. The positions of O2 and O3 are described as $(x_{av} + \delta x, x_{av} + \delta x, 0)$ and $(x_{av} + \delta x, -x_{av} - \delta x, 0)$, respectively, where x_{av} is the

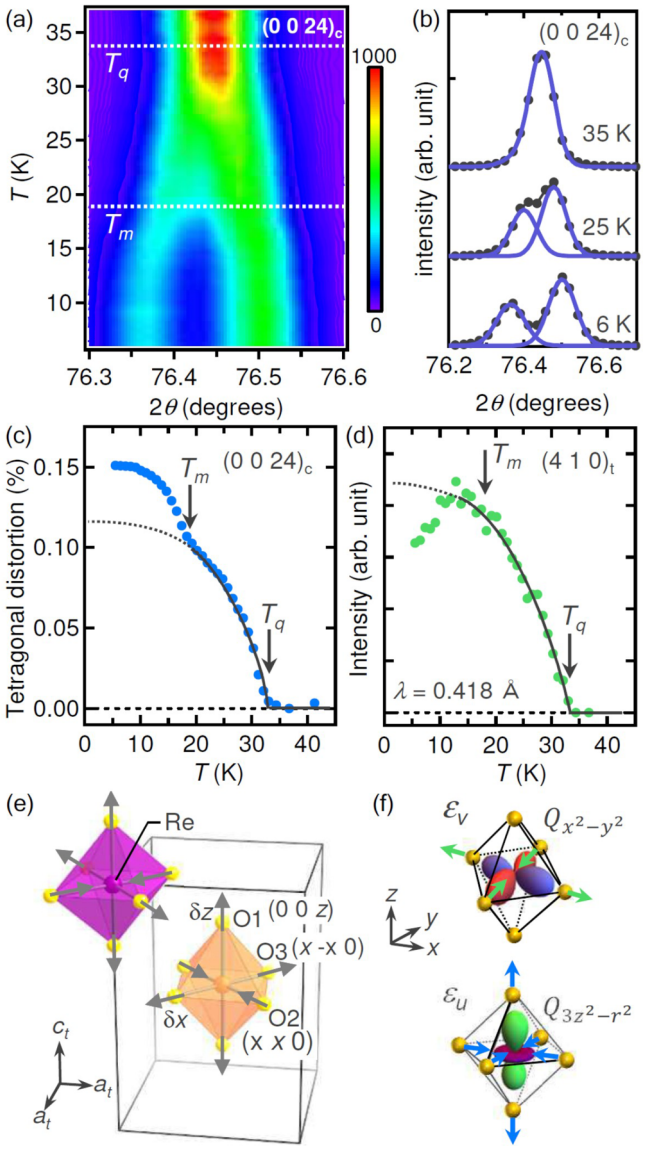

FIG. 2. (a) Temperature evolution of the synchrotron XRD intensity of the $(0\,0\,2\,4)_c$ reflection measured at an off-resonant condition ($E = 29.65$ keV) on a single crystal of Ba_2MgReO_6. (b) Fittings of the $(0\,0\,2\,4)_c$ reflection with double Gaussian functions to obtain the tetragonal distortion, $c_t - \sqrt{2}a_t$ as shown for the typical 6-, 25-, and 35-K data. Temperature dependences of (c) the tetragonal distortion and (d) the integrated intensity of the $(4\ 1\ 0)_t$ reflection. The black lines are visual guides. (e) Schematics of the structural deformation observed below T_q. The ReO_6 octahedra at $z = 0$ and 1/2 are shown by purple and orange colors, respectively. There are three types of oxygen sites, O1, O2, and O3, in the low-temperature tetragonal $P4_2/mnm$ structure. The gray arrows show displacements of the oxygen atoms. (f) Schematic of the quadrupolar moments $Q_{x^2-y^2}$ and $Q_{3z^2-r^2}$, which couple with the ε_v and ε_u displacement modes observed in Ba_2MgReO_6. The green and blue arrows represent the atomic shifts in the ε_v and ε_u modes, respectively.

average x value and δx is the in-plane shift (shown in the Supplemental Material [37]). The intensity of the superlattice peaks is approximately proportional to $(\delta x)^2$. A comparison between the simulated and the observed intensities provides an approximate estimate for δx at 6 K of 0.022 Å.

The distortion of an octahedron, shown in Fig. 2(e), is described by a combination of two normal modes of an octahedron ε_u and ε_v, which are depicted in Fig. 2(f) (also in the Supplemental Material [37]). Among the dipole, quadrupole, and octupole moments originating from the $J_{\rm eff} = 3/2$ quartet [13], only a quadrupole moment, which is an anisotropic distribution of electronic charge, can induce lattice distortion by a linear coupling through electron-phonon interactions. The quadrupole moments in an octahedral field are classified into two-dimensional $\Gamma_3(Q_{x^2-y^2}, Q_{3z^2-r^2})$ and three-dimensional Γ_5 (Q_{xy}, Q_{yz}, Q_{zx}) representations, which are analogous to the e_g and t_{2g} orbitals of the $3d$ electron, respectively. Among these moments, only the former quadrupolar moments are compatible with the observed lattice distortions: In other words, only $Q_{x^2-y^2}$ and $Q_{3z^2-r^2}$ can linearly couple with ε_v and ε_u, respectively [Fig. 2(f)]. The fact that the two distortions take place simultaneously in one octahedron means that the quadrupole moment is a linear combination of the $Q_{x^2-y^2}$ and $Q_{3z^2-r^2}$ moments. The $Q_{x^2-y^2}$ component may be predominant because the amplitude of the ε_v mode [0.044(5) Å] is four times as large as that of the ε_u mode [0.01(1) Å] at 6 K (Supplemental Material [37]). Note that the ε_v distortion is uniform in a layer and stacks in a staggered manner along the c axis, whereas the ε_u distortion is common for all the ReO_6 octahedra [Fig. 2(e)]. This result indicates an antiferroic alignment of the $Q_{x^2-y^2}$ moment and a ferroic alignment of the $Q_{3z^2-r^2}$ moment as depicted in Fig. 3. Thus, we conclude that below T_q, quadrupolar order composed of antiferroically arranged $Q_{x^2-y^2}$ moments and ferroically arranged $Q_{3z^2-r^2}$ is created in Ba_2MgReO_6.

According to the previous theoretical calculations on the electronic orders of the $5d^1$ DPs [13], three types of interactions between the spin-orbit-entangled electrons are considered: the nearest-neighbor antiferromagnetic exchange J, the nearest-neighbor ferromagnetic exchange J', and the electric quadrupolar interaction V. Canted antiferromagnetic magnetic order with a large ferromagnetic moment along $[1\ 1\ 0]_c$ observed in Ba_2MgReO_6 [26] and Ba_2NaOsO_6 [22] is theoretically predicted to be the ground state for relatively large values of V/J and J'/J. In addition, it has been predicted that a quadrupolar order spreads at higher temperatures above this magnetic order as shown in the phase diagram (Fig. 3) [8,13]. Thus, starting from a the disordered state of the quartet, successive transitions occur upon cooling first by removing the quadrupolar degree of freedom and then by removing the dipolar degree of freedom; these transitions are of second order. Our observations for Ba_2MgReO_6 are consistent with the theoretical predictions.

Anomalies in the temperature dependences of the tetragonality and the superlattice intensity at T_m, shown in Figs. 2(c) and 2(d), are reasonably explained within the same theory. When the dipolar order occurs at T_m, other multipolar moments, such as octupolar and quadrupolar moments, are expected to be induced simultaneously [13]. The former does not cause lattice distortion, whereas a quadrupolar moment can induce the distortion of the ReO_6 octahedra. The experimental observations that the tetragonality is increased and the intensity of the $(4\ 1\ 0)_t$ superlattice reflection is decreased below T_m indicate that the $Q_{3z^2-r^2}$ component is enhanced whereas the $Q_{x^2-y^2}$ component is reduced as the result of the dipolar order. Similar behavior is observed for $3d$ TM compounds with Kugel'-Khomskii couplings [41]; an antiferromagnetic order competes with a ferroic quadrupolar order and prefers an antiferroic one. Thus, antiferroically arranged $Q_{x^2-y^2}$ moments are decreased whereas ferroically arranged $Q_{3z^2-r^2}$ moments are increased with developing the antiferromagnetic order in Ba_2MgReO_6.

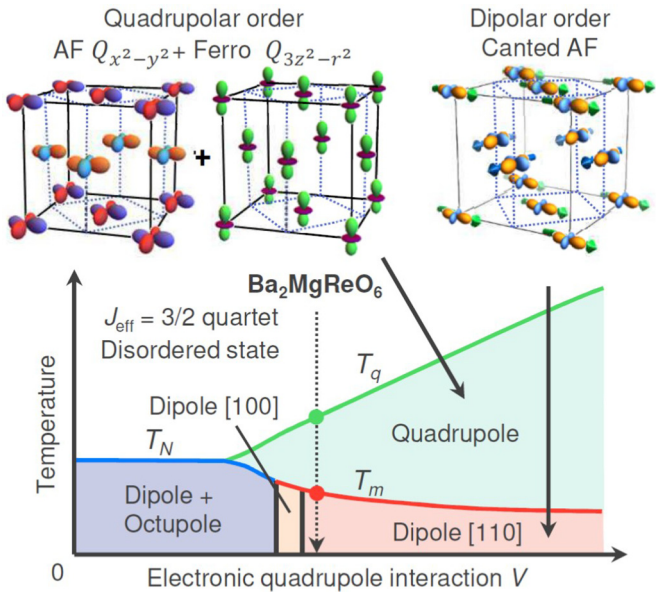

FIG. 3. Observed quadrupolar and dipolar order patterns in Ba_2MgReO_6 and schematic mean-field phase diagram for a d^1 double perovskite with the $J_{\rm eff} = 3/2$ quartet state at $J'/J = 0.2$ is depicted as a function of the electric quadrupole interaction V [8,13]. "Dipole [1 1 0]" and "dipole [1 0 0]" refer to the two-sublattice magnetic orders with the net magnetic moments along the $[1\ 1\ 0]_c$ and $[1\ 0\ 0]_c$ axes, respectively. Quadrupole and dipole + octupole refer to multipole orders of quadrupoles and of both dipoles and octupoles, respectively.

There is one notable discrepancy between our experimental results for Ba_2MgReO_6 and the theoretical prediction of the quadrupolar order [13]. We find a quadrupolar order with a linear combination of the $Q_{x^2-y^2}$ and $Q_{3z^2-r^2}$ moments below T_q, whereas the theory predicts a simple antiferroic quadrupolar order of purely $Q_{x^2-y^2}$ moments. A similar type of quadrupolar (orbital) order with two components occurs in $LaMnO_3$ where electron-phonon couplings and lattice anharmonicity induce ferroic quadrupolar moments in the antiferroic quadrupolar order [42–44]. It is plausible that electron-phonon couplings, which are not considered in the theoretical calculation, and other effects, such as quantum fluctuations, would play a role in stabilizing the $Q_{x^2-y^2}$-$Q_{3z^2-r^2}$ quadrupolar order in Ba_2MgReO_6.

In conclusion, our study establishes the existence of successive phase transitions to multipolar orders for the

correlated spin-orbit-entangled 5*d* electrons in the DP Ba_2MgReO_6. Our observation is consistent with the mean-field theory for spin-orbit-entangled electrons. Therefore, Ba_2MgReO_6 provides an opportunity to experimentally investigate the symmetry breaking of the multipolar degree of freedom in 5*d* electron systems.

In future studies, the detection of elementary excitation from these multipolar orders must be of great interest and importance in capturing the dynamics of multipoles [45,46]. Understanding the nature of interactions between multipolar moments would help us to explore an exotic superconductivity mediated by multipolar fluctuations [47] and quantum liquid states of spin-orbit-entangled electrons [48,49].

The authors are grateful to R. Kurihara for insightful discussions. This work was partly supported by Japan Society for the Promotion of Science (JSPS) KAKENHI Grants No. JP18K13491, No. JP18H04308 (J-Physics), and No. JP19H05826 and by the Core-to-Core Program (A) Advanced Research Networks. G.C. was supported by GRF Grant No.17303819 from RGC of Hong Kong. The synchrotron radiation experiments at BL19LXU in SPring-8 were performed with the approval of RIKEN (Proposal No. 20180095). The off-resonant XRD experiments in the High Energy Accelerator Research Organization (KEK) were performed under the approval of the Photon Factory Program Advisory Committee (Proposal No. 2019G145).

[1] J. G. Bednorz and K. A. Muller, Z. Phys. B: Condens. Matter **64**, 189 (1986).
[2] E. Dagotto, Rev. Mod. Phys. **66**, 763 (1994).
[3] A. P. Ramirez, J. Phys.: Condens. Matter **9**, 8171 (1997).
[4] Y. Tokura, Rep. Prog. Phys. **69**, 797 (2006).
[5] N. Grewe and F. Steglich, *Handbook on the Physics and Chemistry of Rare Earths* (Elsevier, Amsterdam, 1991), Vol. 14. p. 343.
[6] A. C. Hewson, *The Kondo Problem to Heavy Fermions* (Cambridge University Press, Cambridge, UK, 1997).
[7] D. Pesin and L. Balents, Nat. Phys. **6**, 376 (2010).
[8] W. Witczak-Krempa, G. Chen, Y. B. Kim, and L. Balents, Annu. Rev. Condens. Matter Phys. **5**, 57 (2014).
[9] J. G. Rau, E. K.-H. Lee, and H.-Y. Kee, Annu. Rev. Condens. Matter Phys. **7**, 195 (2016).
[10] B. J. Kim, H. Jin, S. J. Moon, J.-Y. Kim, B.-G. Park, C. S. Leem, J. Yu, T. W. Noh, C. Kim, S.-J. Oh, J.-H. Park, V. Durairaj, G. Cao, and E. Rotenberg, Phys. Rev. Lett. **101**, 076402 (2008).
[11] B. J. Kim, H. Ohsumi, T. Komesu, S. Sakai, T. Morita, H. Takagi, and T. Arima, Science **323**, 1329 (2009).
[12] G. Jackeli and G. Khaliullin, Phys. Rev. Lett. **102**, 017205 (2009).
[13] G. Chen, R. Pereira, and L. Balents, Phys. Rev. B **82**, 174440 (2010).
[14] J. Romhányi, L. Balents, and G. Jackeli, Phys. Rev. Lett. **118**, 217202 (2017).
[15] H. Kusunose, J. Phys. Soc. Jpn. **77**, 064710 (2008).
[16] J. A. Mydosh and P. M. Oppeneer, Rev. Mod. Phys. **83**, 1301 (2011).
[17] A. S. Patri, A. Sakai, S. Lee, A. Paramekanti, S. Nakatsuji, and Y. B. Kim, Nat. Commun. **10**, 4092 (2019).
[18] S. Vasala and M. Karppinen, Prog. Solid State Chem. **43**, 1 (2015).
[19] A. Paramekanti, D. D. Maharaj, and B. D. Gaulin, Phys. Rev. B **101**, 054439 (2020).
[20] K. E. Stitzer, M. D. Smith, and H. C. Zur Loye, Solid State Sci. **4**, 311 (2002).
[21] A. S. Erickson, S. Misra, G. J. Miller, R. R. Gupta, Z. Schlesinger, W. A. Harrison, J. M. Kim, and I. R. Fisher, Phys. Rev. Lett. **99**, 016404 (2007).
[22] L. Lu, M. Song, W. Liu, A. P. Reyes, P. Kuhns, H. O. Lee, I. R. Fisher, and V. F. Mitrović, Nat. Commun. **8**, 14407 (2017).
[23] K. Willa, R. Willa, U. Welp, I. R. Fisher, A. Rydh, W.-K. Kwok, and Z. Islam, Phys. Rev. B **100**, 041108(R) (2019).
[24] M. A. de Vries, A. C. Mclaughlin, and J.-W. G. Bos, Phys. Rev. Lett. **104**, 177202 (2010).
[25] C. A. Marjerrison, C. M. Thompson, G. Sala, D. D. Maharaj, E. Kermarrec, Y. Cai, A. M. Hallas, M. N. Wilson, T. J. S. Munsie, G. E. Granroth, R. Flacau, J. E. Greedan, B. D. Gaulin, and G. M. Luke, Inorg. Chem. **55**, 10701 (2016).
[26] D. Hirai and Z. Hiroi, J. Phys. Soc. Jpn. **88**, 064712 (2019).
[27] D. D. Maharaj, G. Sala, M. B. Stone, E. Kermarrec, C. Ritter, F. Fauth, C. A. Marjerrison, J. E. Greedan, A. Paramekanti, and B. D. Gaulin, Phys. Rev. Lett. **124**, 087206 (2020).
[28] H. Ishikawa, T. Takayama, R. K. Kremer, J. Nuss, R. Dinnebier, K. Kitagawa, K. Ishii, and H. Takagi, Phys. Rev. B **100**, 045142 (2019).
[29] K. G. Bramnik, H. Ehrenberg, J. K. Dehn, and H. Fuess, Solid State Sci. **5**, 235 (2003).
[30] A. Abragam and B. Bleaney, *Electron Paramagnetic Resonance of Transition Ions* (Oxford University Press, Oxford/New York, 1970).
[31] M. Yabashi, T. Mochizuki, H. Yamazaki, S. Goto, H. Ohashi, K. Takeshita, T. Ohata, T. Matsushita, K. Tamasaku, Y. Tanaka, and T. Ishikawa, Nucl. Instruments Methods Phys. Res., Sect. A **467-468**, 678 (2001).
[32] M. Blume, J. Appl. Phys. **57**, 3615 (1985).
[33] Y. Murakami, J. P. Hill, D. Gibbs, M. Blume, I. Koyama, M. Tanaka, H. Kawata, T. Arima, Y. Tokura, K. Hirota, and Y. Endoh, Phys. Rev. Lett. **81**, 582 (1998).
[34] X. Liu, T. Berlijn, W.-G. Yin, W. Ku, A. Tsvelik, Y.-J. Kim, H. Gretarsson, Y. Singh, P. Gegenwart, and J. P. Hill, Phys. Rev. B **83**, 220403(R) (2011).
[35] D. Okuyama, Y. Tokunaga, R. Kumai, Y. Taguchi, T. Arima, and Y. Tokura, Phys. Rev. B **80**, 064402 (2009).
[36] H. Sagayama, S. Toyoda, K. Sugimoto, Y. Maeda, S. Yamada, and T. Arima, Phys. Rev. B **90**, 241113(R) (2014).
[37] See Supplemental Material at http://link.aps.org/supplemental/10.1103/PhysRevResearch.2.022063 for the details of polarization analysis and energy dependence of magnetic reflections observed in the resonant x-ray scattering experiments and structural analysis using the off-resonant x-ray-diffraction data.
[38] H. Ishizuka and L. Balents, Phys. Rev. B **90**, 184422 (2014).
[39] K. Yamamura, M. Wakeshima, and Y. Hinatsu, J. Solid State Chem. **179**, 605 (2006).

[40] *International Tables for Crystallography. Volume A, Space-Group Symmetry*, Fifth, revised ed., edited by T. Hahn (Kluwer Academic, Dordrecht/London, 2002).
[41] K. I. Kugel' and D. I. Khomskii, Sov. Phys. Usp. **25**, 231 (1982).
[42] J. Kanamori, J. Appl. Phys. **31**, S14 (1960).
[43] J. Rodríguez-Carvajal, M. Hennion, F. Moussa, A. H. Moudden, L. Pinsard, and A. Revcolevschi, Phys. Rev. B **57**, R3189 (1998).
[44] E. Pavarini and E. Koch, Phys. Rev. Lett. **104**, 086402 (2010).
[45] G. Jackeli and G. Khaliullin, Phys. Rev. Lett. **103**, 067205 (2009).
[46] W. M. H. Natori, M. Daghofer, and R. G. Pereira, Phys. Rev. B **96**, 125109 (2017).
[47] S. Sumita, T. Nomoto, and Y. Yanase, Phys. Rev. Lett. **119**, 027001 (2017).
[48] W. M. H. Natori, E. C. Andrade, and R. G. Pereira, Phys. Rev. B **98**, 195113 (2018).
[49] M. G. Yamada, M. Oshikawa, and G. Jackeli, Phys. Rev. Lett. **121**, 097201 (2018).